

Three Branches of Dynamo Action

Emmanuel Dormy^{1‡}, Ludivine Oruba^{2,3} and Ludovic
Petitdemange^{2,3}

¹Department of Mathematics & Applications, CNRS UMR 8553, Ecole Normale Supérieure, Paris, France

²Physics Department, Ecole Normale Supérieure, Paris, France

³LERMA, CNRS UMR 8112, Observatoire de Paris, Paris, France

E-mail: dormy@dma.ens.fr

Abstract.

In addition to the weak-dipolar state and to the fluctuating-multipolar state, widely discussed in the literature, a third regime has been identified in (Dormy 2016). It corresponds to a strong-dipolar branch which appears to approach, in a numerically affordable regime, the magnetostrophic limit relevant to the dynamics of the Earth's core. We discuss the transitions between these states and point to the relevance to this strong-dipolar state to Geodynamo modelling.

Keywords: Dynamo action, Magnetostrophic balance, Dynamo bifurcation.

1. Introduction

The Earth’s magnetic field is sustained by self-exciting dynamo action in the liquid core of our planet. Part of the kinetic energy of the flow is transferred to magnetic energy. In fact, in the Earth’s core, most of the energy is anticipated to be dissipated by electrical currents. We describe here the existing numerical models and show how they appear to fall into three distinct branches characteristic of different forces balances.

Since the first full numerical models of dynamo action (Zhang & Busse 1988, Zhang & Busse 1989, Glatzmaier & Roberts 1995), many parameter space surveys have been performed. This has allowed to produce phase-diagrams which, depending on the controlling parameters, describe which dynamo states can be achieved. Wide parameters surveys (e.g. Christensen & Aubert 2006, Schinnerer et al. 2012) clearly identified two branches of dynamo action. The first one is characterised by a dominant axial dipole, while the second one, at larger forcing, is largely multipolar, with a fluctuating dipolar component. It was shown (Simitev & Busse 2009) that the transition between these two dynamo states can be hysteretic if stress-free boundary conditions were considered.

Sadly, upon closer investigation none of these two states turned out to be relevant for the Geodynamo. The first state, characterised by a dominant axial dipole, was shown to be largely controlled by viscous effects (King & Buffett 2013, Oruba & Dormy 2014*a*), and the second one to involve significant inertial effects (Christensen & Aubert 2006, Schinnerer et al. 2012, Oruba & Dormy 2014*b*).

The Earth rotates with one revolution per day, given the viscosity of liquid iron at these temperature and pressure (see de Wijs et al. 1998), we can easily conclude that viscous effects will only become relevant at very small scales. A naive dimensional analysis approach yields $\ell_v^2 \sim \nu/\Omega$. Asymptotic developments (e.g. Dormy & Soward 2007) reveal more elaborate scalings of the form $\ell_v^\alpha \sim \nu/\Omega L^{\alpha-2}$ (where L denotes the typical size of the Earth’s core). The first relevant length scale for a vertical shear, for example, corresponds to $\alpha = 3$. For geophysically relevant estimates, these length scales would be of a few meters, less than a kilometer. Length scales which lie below the resolution of current numerical models.

Typical velocities in the Earth’s core can be inferred from the secular variation of the magnetic field (Holme 2007), this yields $U \simeq 10^{-4} \text{m s}^{-1}$. There again, dimensional analysis reveals the length scale at which inertial effects will be comparable to the effects of global rotation (the so-called Rossby radius), $\ell_I \sim U/\Omega$, again of the order of a few meters. So that inertial effects are not expected to play a significant role, on the time scale of secular variation, at the large spatial scale.

The relevant balance for the Earth’s core is therefore one in which both viscous effects and inertial effects are negligible on the large scales. This is known as the magnetostrophic balance (see Moffatt 1978). The issue of whether the limit system of equations (i.e. omitting both the viscous term and the inertial term in the governing equations) is well posed is a challenging one. First put forward by Taylor in 1963 (Taylor 1963), this system proved extremely difficult to solve numerically. The well-

posedness of this limit raises complicated mathematical issues (Gallagher & Gérard-Varet 2016). A first set of solutions in the case of an axi-symmetric configuration has however recently been achieved (Roberts & Wu 2014, Wu & Roberts 2015).

We here take the simpler point of view of retaining all the terms in the equations, but vary the parameters, so as to try and approach a magnetostrophic equilibrium. The crucial issue in doing so, is to assess that inertial and viscous effects are indeed small in the realised solution. To that end, a useful tool is to study the bifurcation diagram for various choices of the parameters, the different branches on this diagram naturally corresponding to different forces balances. The bifurcation diagram for dynamo action in the limit relevant to the Earth’s core has been the focus of many analytical or mixed analytical-numerical studies (Eltayeb & Roberts 1970, Childress & Soward 1972, Soward 1974, Fautrelle & Childress 1982, Roberts 1988). The main result is that the bifurcation diagram should consist of two branches. The first branch necessarily involves significant viscous effects and is referred to as the “weak-field” branch. On this branch, viscous effects are necessary to allow deviation from the Proudman-Taylor constraint (i.e. the tendency for the flow in a rapidly rotating reference frame to be independent on the coordinate in the direction of the axis of rotation). The flow will thus develop short length scales in the directions orthogonal to the axis of rotation. The most obvious of these length scales involving an $E^{1/3}$ dependence (see Dormy & Soward 2007, for example). As the strength of convection increases, both the flow and the field gain in amplitude. A transition, characterised by a turning point, is anticipated when the Lorentz force becomes large enough. When this turning point is reached, the weak-field solution becomes unstable, and the magnetic field experiences a runaway amplification. Saturation will be achieved when the field reaches a strength sufficient for the Lorentz force to be comparable with the Coriolis force. This second branch is referred to as the “strong-field” branch. On this branch the amplitude of the Lorentz force is comparable to that of the Coriolis force.

The above description was so far disconnected from direct numerical simulations of spherical dynamos. Recently, however, Dormy (2016) pointed out the existence of a third dynamo state, numerically achievable at the cost of an under-estimated magnetic diffusivity. This regime appears to approach the relevant magnetostrophic force balance. This strong-dipolar dynamo state, described numerically, is characterised by an hysteresis with respect to the viscous-state. The transition occurs at a turning point, which is characterised by a runaway field growth. This bifurcation sequence establishes a first connection between direct numerical models and earlier asymptotic developments.

In this article, we will rapidly review the available results on dynamo states available from numerical simulations. We further investigate the numerical strong-dipolar (SD) branch, describe its relation with the earlier theoretical bifurcation sequence, and ponder on the relevance of the strong-dipolar state to the Geodynamo.

2. Governing equations

Let us start by introducing the standard mathematical model for the Geodynamo. The numerical simulations discussed in this paper are restricted Boussinesq models. The computational domain consists of a spherical shell with aspect ratio $r_i/r_o = 0.35$. The flow is thermally driven, and a fixed difference of temperature is imposed between the inner and outer boundaries. It should be noted, that in the Earth's core, buoyancy effects are associated with both thermal and compositional effects. The simplest form of governing equations is however similar in both cases (see Braginsky & Roberts 1995, for a detailed discussion). All the simulations used in this work rely on no-slip mechanical boundary conditions as well as an insulating outer domain. The inner core is insulating in most simulations, and a few simulations involve a conducting inner core with the same conductivity as the fluid.

The governing equations in the rotating frame of reference can then be written in their non-dimensional form – using $L = r_o - r_i$ as unit of length, L^2/η as unit of time, ΔT as unit of temperature, and $(\rho\mu\eta\Omega)^{1/2}$ as unit for the magnetic field – as

$$E_\eta [\partial_t \mathbf{u} + (\mathbf{u} \cdot \nabla) \mathbf{u}] = -\nabla \pi + E \Delta \mathbf{u} - 2\mathbf{e}_z \times \mathbf{u} + \text{Ra} \, \mathbf{q} T \mathbf{r} + (\nabla \times \mathbf{B}) \times \mathbf{B}, \quad (1)$$

$$\partial_t \mathbf{B} = \nabla \times (\mathbf{u} \times \mathbf{B}) + \Delta \mathbf{B}, \quad \partial_t T + (\mathbf{u} \cdot \nabla) T = \mathbf{q} \Delta T, \quad (2)$$

$$\text{with} \quad \nabla \cdot \mathbf{u} = \nabla \cdot \mathbf{B} = 0. \quad (3)$$

System (1–3) involves four independent non-dimensional parameters, which are the Ekman number $E = \nu/(\Omega L^2)$, the magnetic Ekman number $E_\eta = \eta/(\Omega L^2)$, the Roberts number $\mathbf{q} = \kappa/\eta$, and the modified Rayleigh number $\text{Ra} = \alpha g \Delta T L / (\kappa \Omega)$, in which ν is the kinematic viscosity of the fluid, α the coefficient of thermal expansion, g is the gravity at the outer bounding sphere (the gravity profile is linear in radius), κ its thermal diffusivity, and η its magnetic diffusivity. The modified Rayleigh number Ra , as defined above, differs from its most classical definition $\alpha g \Delta T L^3 / (\nu \kappa)$, to which it is related via an Ekman factor. Whereas the later is the relevant parameter to measure energy input in the standard Rayleigh-Bénard setup, it is not any longer relevant in the magnetostrophic limit.

The above four independent parameters are enough to fully define the system. We shall now consider the relevant values of these parameters for the Earth's core. The orders of magnitude of the dimensional coefficients outlined in the introduction reveal

$$E \simeq 10^{-15}, \quad E_\eta \simeq 10^{-9}, \quad \mathbf{q} \simeq 10^{-5}. \quad (4)$$

The last non-dimensional parameter, Ra , controlling the strength of thermal convection is difficult to quantify in a Boussinesq formalism. While the heat gradient across the core is of the order of 10^3 K, most of the heat in the actual core is carried along the adiabat. Only the super-adiabatic gradient is relevant in the Boussinesq framework. This deviation is only of the order of 10^{-3} K (see Gubbins 2001, Jones 2011), so difficult to estimate with great precision. This results in the following estimate for our definition of the Rayleigh number $\text{Ra} \simeq 10^{13}$ (Gubbins 2001). Obviously this value should be large

enough, so that, even though q is a vanishing number, the product $\widetilde{Ra} = Ra q$ remains of order unity. The above estimate yields $\widetilde{Ra} \simeq 10^8$.

The non-dimensional form chosen in (1–3), often referred to as the “strong-field scaling”, highlights the primary magnetostrophic balance (order one terms) and the three vanishing parameters (4). The Taylor state introduced above (Taylor 1963) amounts to dropping all small terms in (1–3). The only parameter left to control this limit system is then the modified Rayleigh number \widetilde{Ra} . So that the strength of the magnetic field in this limit should depend on this sole parameter.

It is worth pondering on the ratios of the small terms in (1–3). The ratio of the Ekman number to the magnetic Ekman number defines the magnetic Prandtl number $Pm = E/E_\eta$, this defines the ratio of two small parameters (vanishing in the geophysically relevant magnetostrophic limit), but as we shall see controlling this ratio in the limiting process is essential. The ratio of the magnetic Prandtl number to the Roberts number defines the classical hydrodynamic Prandtl number, $Pr = Pm/q$. There again, both Pm and q are small numbers, but their ratio remains an important quantity.

The importance of the ratio of small parameters in a double (or even tripple in our case) limit, will not come as a surprise to the mathematical community. Besides, its importance has recently been stressed in physical applications when considering the saturation properties of MHD turbulence (Fromang & Papaloizou 2007, Fromang et al. 2007).

Our analysis is tested against a wide numerical database corresponding to some 300 direct numerical simulations. The data sample is composed of 180 runs kindly provided by U. Christensen, and of additional runs, either previously reported in Morin & Dormy (2009), Schrunner et al. (2012) and Dormy (2016), or presented in Table 1.

3. The Weak-Dipolar dynamo state

The first and most documented dynamo state is for obvious reason the dipolar state. Dynamos in this state have been reported since the very early days of dynamo modelling. Owing to their dipolar nature, these models have even often been argued to be relevant to the Geodynamo. It is now evident that viscous effects are present at leading order in the forces balances.

This branch is the first dynamo mode produced as the modified Rayleigh \widetilde{Ra} is increased away from its critical value for the onset of convection \widetilde{Ra}_c (which can itself be subcritical (see Guervilly et al. 2015)). The onset of dynamo action, or dynamo bifurcation, has been carefully investigated in Morin & Dormy (2009). Depending on the parameters being considered, they reported either super-critical, sub-critical or isola branches for the onset of dynamo action (see figure 1). It is important to stress that each point on these numerical bifurcation diagrams corresponds to a time averaged fully three-dimensional simulation.

The Ekman number was varied between 10^{-3} and 10^{-4} , and the bifurcation type over this range appears to depend only on the parameter E_η . Super-critical bifurcations

were obtained for both $E = 3 \times 10^{-4}$ and $E = 10^{-4}$, with $E_\eta < 5 \times 10^{-5}$; Sub-critical bifurcations for both $E = 3 \times 10^{-4}$ and $E = 10^{-4}$, with $5 \times 10^{-5} < E_\eta < 2 \times 10^{-4}$; and Isola were obtained for both $E = 10^{-3}$ and $E = 3 \times 10^{-4}$ with $E_\eta > 2 \times 10^{-4}$. These simulations were all performed at fixed $\text{Pr} = E E_\eta^{-1} \text{q}^{-1} = 1$.

The physical explanation for this change of behaviour has not been achieved so far, but the ordering highlighted above points to the importance of inertial effects in controlling the nature of the transition.§

The importance of the flow helicity on the dynamo generation mechanism for this dynamo state has been highlighted by Olson et al. (1999). Besides, Sreenivasan & Jones (2011) argue that kinematic helicity enhancement by the magnetic field could provide a mechanism for the occurrence of sub-critical dynamo branches.

The importance of viscous forces in this dynamo branch has long been overlooked. It was however recently pointed out (King & Buffett 2013) that the typical length scale of the flow exhibits a clear $E^{1/3}$ dependence, characteristic as explained above of the viscous-Coriolis dominant force balance.

We present in figure 2 three different length scales. The first one, $\ell_{u\text{peak}}$, is defined by considering the time averaged kinetic energy spectrum. It is defined as $\ell_{u\text{peak}} = \pi/l_{\text{peak}}$ where l_{peak} corresponds to the spherical harmonic degree for the peak of the energy spectrum. The second length scale $\ell_{u\text{CA06}}$ corresponds to the length scale defined in Christensen & Aubert (2006) and used in King & Buffett (2013), it is defined as $\ell_{u\text{CA06}} = \pi/l_{\text{CA06}}$ where l_{CA06} corresponds to the mean value of the spherical harmonics degree in the time-averaged kinetic energy spectrum (see Christensen & Aubert 2006, equation (27)). The third length scale $\ell_{u\text{vort}}$, introduced by Oruba & Dormy (2014a), is defined as

$$\ell_{u\text{vort}}^2 = \frac{\langle \mathbf{u}^2 \rangle}{\langle (\nabla \times \mathbf{u})^2 \rangle}, \quad (5)$$

where $\langle \cdot \rangle$ denotes time and volume averaged quantities.

Figure 2 highlights that the three typical length scales defined above follow an Ekman dependence characteristic of the viscous, $E^{1/3}$, scaling.

Because viscous forces are important in this branch, and to attempt a link with the earlier asymptotic studies listed above, we will in the sequel refer to this branch as the weak-dipolar (WD) branch. Of course this branch is saturated, and non-linear effects are affecting the flow, both via the non-linear inertial term and via the Lorentz force.

4. From Weak-Dipolar dynamos to Fluctuating-Multipolar dynamos

As the forcing is increased, i.e. as the modified Rayleigh Ra is further increased away from Ra_c , a transition to a fluctuating-multipolar (FM) dynamo state has been initially reported by Kutzner & Christensen (2002) and described in further details in Christensen & Aubert (2006).

§ Note that the original paper (Morin & Dormy 2009) uses a different ordering based on the magnetic Prandtl number at fixed Ekman number.

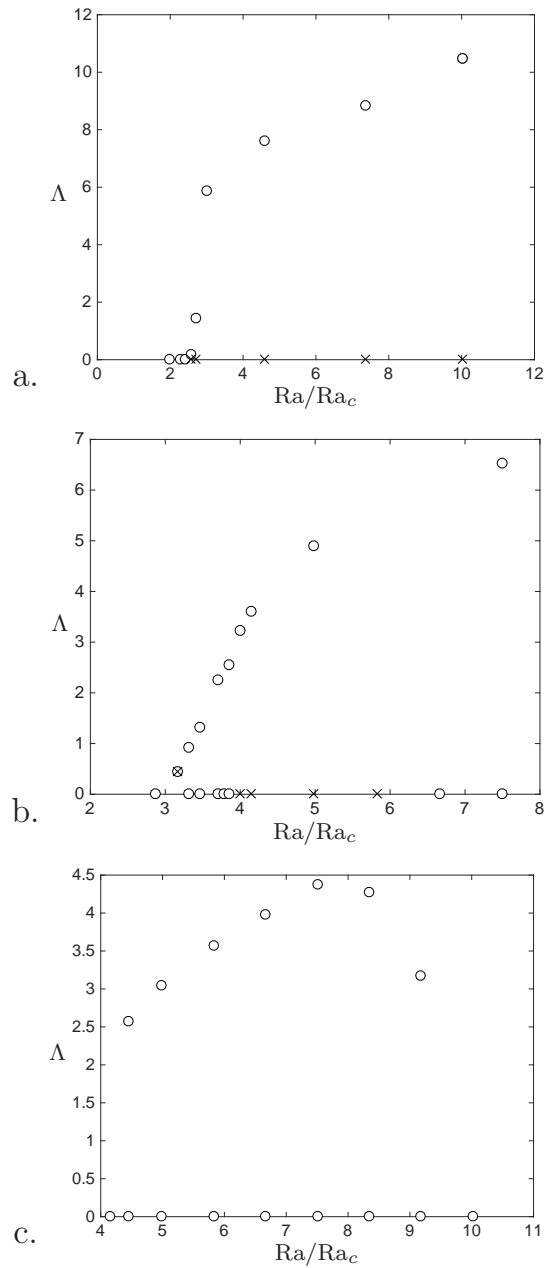


Figure 1. Bifurcation diagrams obtained for $E = 3 \times 10^{-4}$ and (a) $E_\eta = 5 \times 10^{-5}$, (b) $E_\eta = 10^{-4}$, (c) $E_\eta = 2 \times 10^{-4}$ (\circ stable, \times unstable, \otimes meta-stable). These respectively correspond to a super-critical, a sub-critical and an isola bifurcation diagram. The same sequence of transitions between the various bifurcation diagrams were obtained at different values of E , for similar values of E_η (see Morin & Dormy 2009).

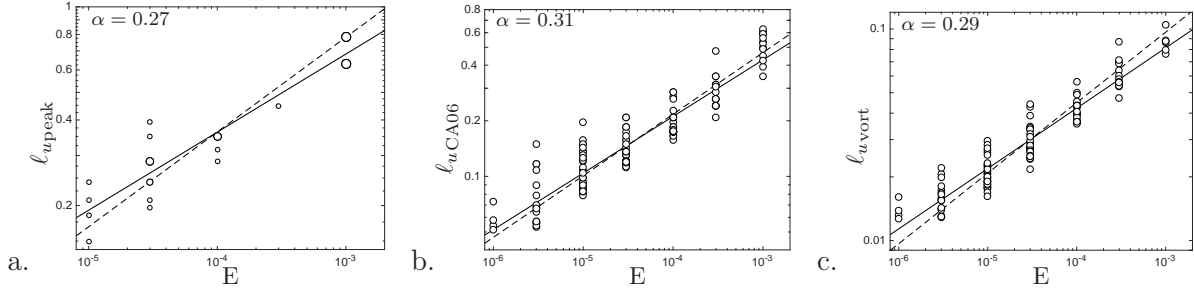


Figure 2. Evolution of the typical length scales of the flow as a function of the Ekman number for dynamo in the weak-dipolar state. (a) The length scale at which the energy spectrum peaks $l_{u\text{peak}}$; (b) the averaged length scale $l_{u\text{CA06}}$; and (c) the vorticity length scale $l_{u\text{vort}}$. The dashed line indicates the $E^{1/3}$ scaling. The best fit, derived from a least squares method, in E^α , is indicated by a solid line, and the corresponding value of α is reported on each panel. On the first graph, larger symbols are used when several dynamos produced the same $l_{u\text{peak}}$.

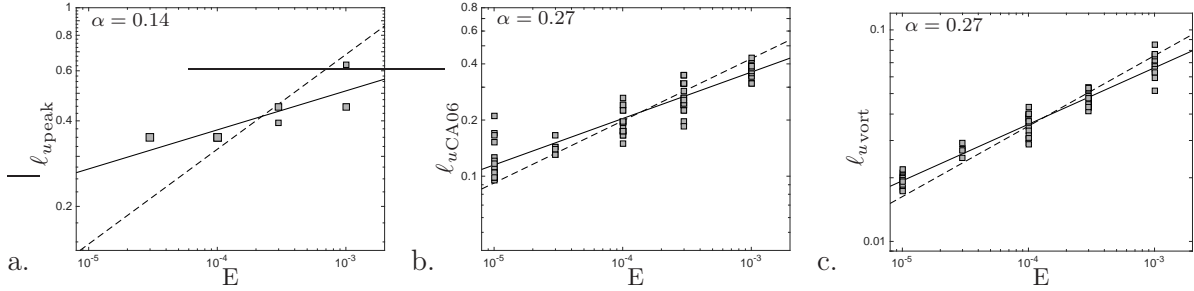


Figure 3. Evolution of the typical length scales of the flow as a function of the Ekman number, same representation as in figure 2, but for numerical dynamos in the multipolar-fluctuating state.

This transition was very early associated with the strength of inertial effects. Indeed Christensen & Aubert (2006) pointed out that the transition was controlled by the “local” Rossby number $\text{Ro}_\ell = U(\Omega l_{u\text{CA06}}^*)^{-1}$ based on the mean velocity length scale $l_{u\text{CA06}}$, defined above (the * denotes dimensional quantities). This clearly indicates that inertial effects become significant at the flow length scale when the weak-dipolar mode is lost. More recently, Oruba & Dormy (2014b) showed that rather than measuring the typical length scale of the realised flow, one could account for the transition with the parameter $\text{Ro} E^{-1/3}$, where $\text{Ro} = U(\Omega L)^{-1}$, because of the above mentioned dependence of the flow length scale as $E^{1/3} L$ in the weak-dipolar branch.

The typical length scales are presented as a function of the Ekman number on figure 3. While the length scales $l_{u\text{vort}}$ and $l_{u\text{CA06}}$ are by construction affected by the viscous dissipation length scale, the length scale $l_{u\text{peak}}$ (corresponding to the energy spectrum peak) exhibits a much weaker dependence on the Ekman number (we stress however the large dispersion due to the small data sample and the difficulty to precisely estimate l_{peak} , which is a small integer). This appears as a signature of inertial effects at the dominant scale of the flow.

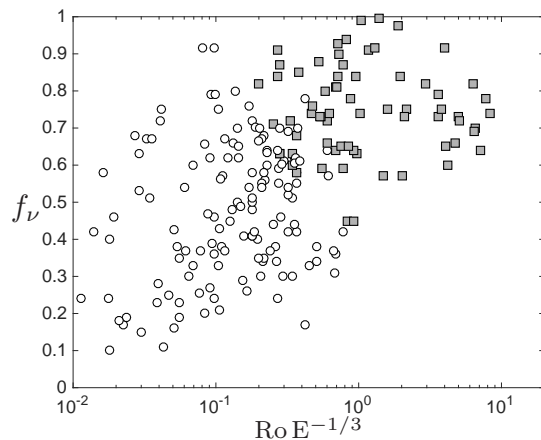


Figure 4. Fraction of viscous dissipation as a function of $\text{Ro} E^{-1/3}$. The transition from the weak-dipolar (circles) to the fluctuating-multipolar state (grey squares) is clearly controlled by $\text{Ro} E^{-1/3}$, characterising the importance of inertial effects at the flow length scale. The fraction of viscous dissipation is significant in both regimes and appears enhanced by inertial effects.

A way to further assess the importance of viscosity is to consider the fraction of energy being dissipated by viscous forces f_ν . The ratio of the energy being dissipated by viscous forces to the total energy dissipation (viscous and ohmic)

$$f_\nu = \frac{E \langle (\nabla \times \mathbf{u})^2 \rangle}{E \langle (\nabla \times \mathbf{u})^2 \rangle + \langle (\nabla \times \mathbf{B})^2 \rangle} = \frac{\rho \nu \langle (\nabla \times \mathbf{u}^*)^2 \rangle}{\rho \nu \langle (\nabla \times \mathbf{u}^*)^2 \rangle + \eta \mu^{-1} \langle (\nabla \times \mathbf{B}^*)^2 \rangle} \quad (6)$$

is reported on figure 4 as a function of the Rossby number based on the viscous scale (Oruba & Dormy 2014b). The relevance of this parameter $\text{Ro} E^{-1/3}$ to distinguish weak-dipolar and fluctuating-multipolar dynamos is evident. We should stress that Schrunner (2013) investigated the behaviour of f_ν (actually $f_{\text{ohm}} = 1 - f_\nu$) and concluded that f_ν was increasing with the local Rossby number, for which $\text{Ro} E^{-1/3}$ offers a very good proxy in the weak-dipolar state.

The fraction of viscously dissipated energy is in general significant in both dynamo states (though some end members models of the weak-dipolar state, reach 10% of viscous dissipation). It is worth noting that this fraction is on average larger in the multipolar regime, for which the field is weaker and the ohmic dissipation is thus lower.

The transition from the weak-dipolar to the fluctuating-multipolar state is illustrated in figure 5. Here again the simulations were performed at fixed $\text{Pr} = E E_\eta^{-1} \text{q}^{-1} = 1$. The two branches are identified with different symbols. These are easily identified by measuring the strength of the dipolar component relative to the total field intensity. The dipolar state is indicated with circles, whereas the fluctuating-multipolar state is indicated with grey squares. In these graphs the magnetic energy density of the non-dimensional magnetic field is reported: $\Lambda = \langle B^2 \rangle / 2$, this corresponds to the Elsasser number. In terms of dimensional variables, this amounts to

$$\Lambda = \langle B^{*2} \rangle / (2\Omega \rho \mu \eta) . \quad (7)$$

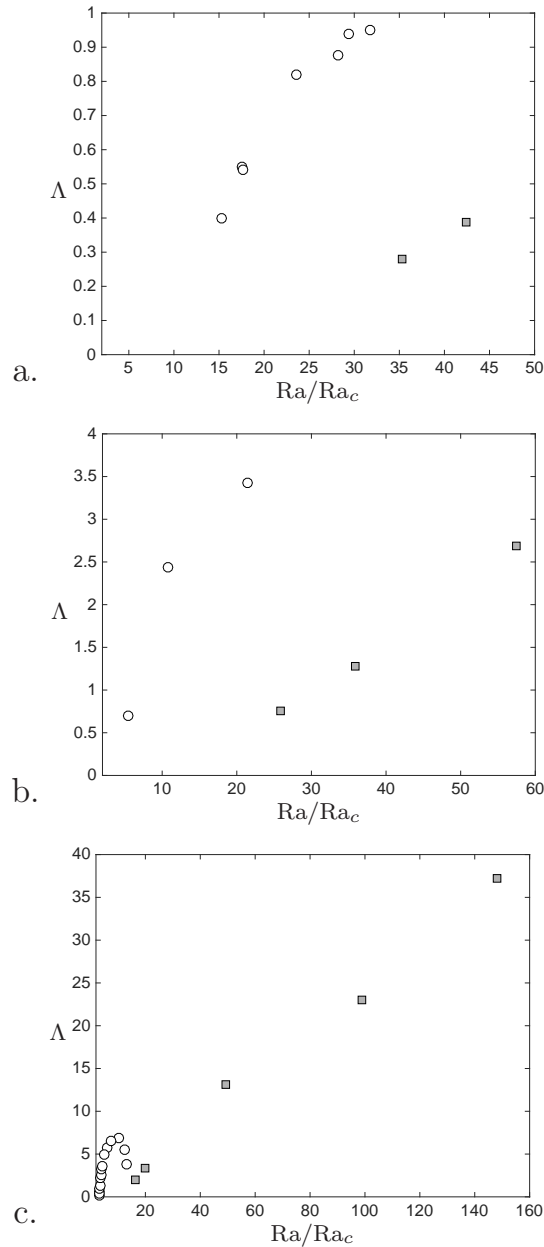


Figure 5. Weak-dipolar (circles) and fluctuating-multipolar (grey squares) branches with no-slip boundary conditions for (a) $E = 3 \times 10^{-5}$, $E_\eta = 1.2 \times 10^{-4}$, $q = 0.25$, (b) $E = 10^{-4}$, $E_\eta = 10^{-4}$, $q = 1$, and (c) $E = 3 \times 10^{-4}$, $E_\eta = 10^{-4}$, $q = 3$.

Figures 5a and 5b highlight the discontinuity in the dynamo branches. Figure 5c shows that for some parameters, the efficiency of the viscous dynamo state starts to decrease before the transition occurs. This highlights that although the primary force balance on this branch involves the viscous term, non-linear effects are important, in saturating the field growth, but also in modifying the flow (which, in this case, provides a lower saturation level at larger forcing).

Non-linear effects in a rotating flow are known to drive zonal flows through the Reynolds stress. Such zonal flows are very weakly damped. If their radial structure

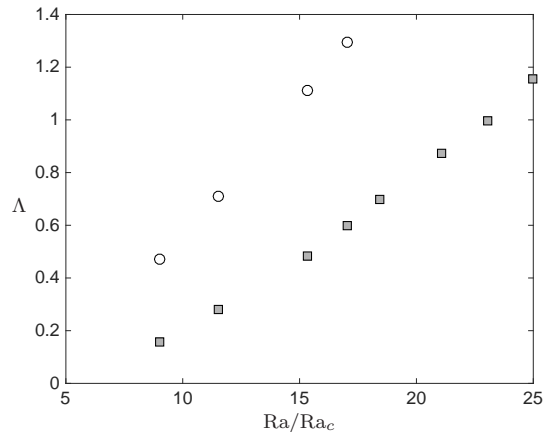


Figure 6. Weak-dipolar (circles) and fluctuating-multipolar (grey squares) branches for $E = 10^{-4}$, $E_\eta = 10^{-4}$, $q = 1$, in the case of stress-free boundary conditions.

is larger than $E^{1/4}L$ they are dominated by boundary layers dissipation (Morin & Dormy 2006). It results that the large-scale zonal flows will behave in a different manner in the case of stress-free boundary conditions (for which only the bulk viscous effects will be relevant). This will, of course be particularly true when the Ekman number is moderately small (as is the case in most numerical models). As the Ekman number decreases, the correction due to the boundary layer dissipation (via Ekman pumping) will become less and less important. For stress-free boundary conditions the possible bistability between the weak-dipolar state and the fluctuating-multipolar state was first highlighted by Simatev & Busse (2009). This is directly associated with the zonal flow, which once present prevents the formation of an organized large-scale field. So that the transition to the fluctuating-multipolar branch is hysteretic and once on this branch, the controlling parameter (the Rayleigh number) can be decreased below the transitional value without recovering the weak-dipolar state. Schrunner et al. (2012) further demonstrated that in this case the controlling parameter was still a local Rossby number, but which needed to be based on the amplitude of the convective flow, and not of the zonal flow itself. This bistability is illustrated by figure 6.

This second dynamo state is characterised by fluctuations of the dipolar component. For this reason, it has sometimes been argued that geomagnetic polarity reversals may be due to the fact the Geodynamo operates near this transition (Olson & Christensen 2006, Christensen 2010). Indeed, an estimation of the parameter $Ro E^{-1/3}$ in the Earth’s core would be very close to the critical value observed in numerical simulations (below, but close to 10^{-1}). It is however most unlikely that the Geodynamo operates on the viscous dipolar branch. The resulting viscous length scale would be extremely small, less than 100 m. The strong-dipolar state described previously is most likely the relevant one, and this transition is probably not relevant to the actual Geodynamo reversals (see discussions in Oruba & Dormy 2014b).

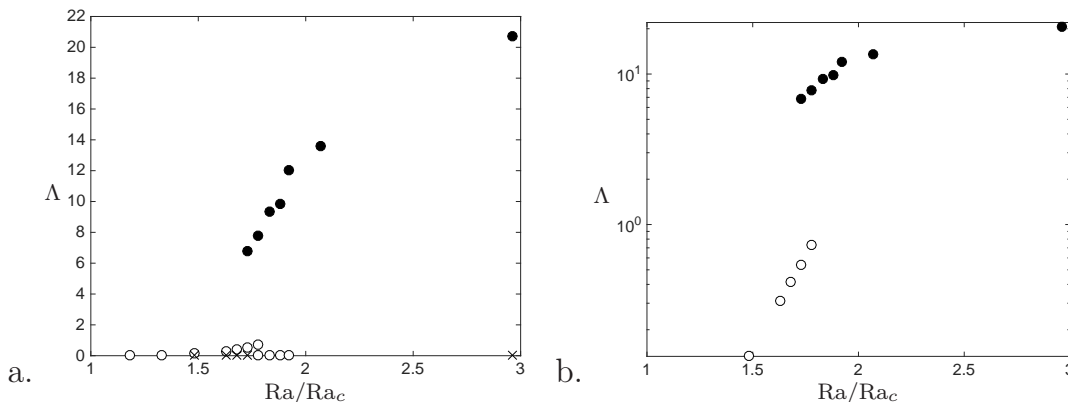


Figure 7. Weak-dipolar (circles) and strong-dipolar (bullets) branches for $E = 3 \times 10^{-4}$, $E_\eta = 1.7 \times 10^{-5}$, $q = 18$. Crosses indicate unstable solutions. The Elsasser number is represented in a linear scale on panel (a) and a log-scale on panel (b), thus highlighting the lower branch.

5. The Strong-Dipolar dynamo state

Recently, Dormy (2016) has shown that if E_η was small enough in the numerical simulations, the viscous-dipolar mode could exhibit a transition to a very different state, of stronger, yet still dipolar, magnetic field. The corresponding bifurcation diagram is illustrated in figure 7. Dormy (2016) pointed that a “cusp catastrophe” occurs in the bifurcation diagram as E_η is decreased at fixed E . This catastrophe accounts for the transition between the single branch reported on figure 1a, yet characterised by a sudden increase near $Ra/Ra_c \simeq 3$, and the turning points highlighted by figure 7.

The Elsasser number Λ is usually assumed to be of order unity in the strong-dipolar state. As can be seen in figure 7, while the values are “of the order of unity” (compared to the extreme values of some parameters, such as those listed in (4)), they are significantly greater than unity. For this reason a modified Elsasser number

$$\Lambda' = \Lambda L / (\text{Rm} \ell_B^*), \quad (8)$$

was used in Dormy (2016), and was shown to offer a closer measurement of the balance between the Coriolis and the Lorentz forces. In the above definition, we used

$$\text{Rm} = \frac{UL}{\eta}, \quad \text{and} \quad \ell_B^2 = \frac{\langle \mathbf{B}^2 \rangle}{\langle (\nabla \times \mathbf{B})^2 \rangle}. \quad (9)$$

Writing in dimensional form the ratio of the Lorentz to the Coriolis force yields

$$\frac{\{(\mu\rho)^{-1} \nabla \times \mathbf{B} \times \mathbf{B}\}}{\{2\boldsymbol{\Omega} \times \mathbf{u}\}} = \frac{B^2}{2\Omega\mu\rho U \ell_B^*}. \quad (10)$$

The classical Elsasser number stems from $U \ell_B^* \simeq \eta$, which is a sensible approximation in an asymptotic sense, as the magnetic Reynolds number is neither very large nor very small in this problem. The modified Elsasser number offers a finer measure of this balance by writing $U \ell_B^* / \eta \simeq \text{Rm} \ell_B^* / L$.

Dormy (2016) has shown that this dynamo state corresponds to a primarily magnetostrophic balance, by comparing the radial components of the curl of the Lorentz

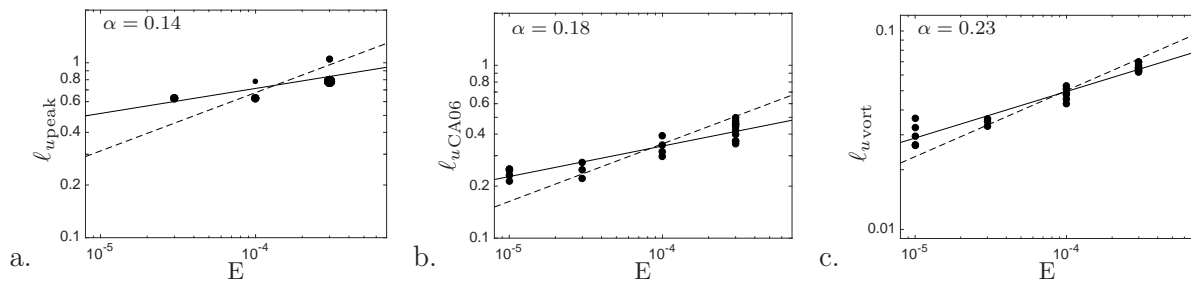


Figure 8. Evolution of the typical length scales of the flow as a function of the Ekman number, same representation as in figure 2, but for numerical dynamos in the strong-dipolar state.

force and the Coriolis force (in order to get rid both of the pressure gradient and of the buoyancy force).

The transition from the viscous-dipolar to the strong-dipolar state, characterised by a runaway field growth, as the turning point of the weak-dipolar state is reached, was also reproduced in Dormy (2016).

6. Geophysical relevance of the strong-dipolar state

We discuss here additional simulations performed in the range $E \in [3 \times 10^{-4}, 10^{-5}]$, $E_\eta \in [1.4 \times 10^{-6}, 2.5 \times 10^{-5}]$, $q \in [5, 18]$ (see Table 1). In these simulations the parameters were chosen such that the strong-field state reported in the previous section was maintained in the limiting process of decreasing both E and E_η . This corresponds to a distinguished limit, relating the small parameters, as introduced in Dormy (2016).

We can first consider, as we did for the first two dynamo states, the length scales dependency with the Ekman number. These are presented in figure 8. While viscosity clearly affects the small length scales of the flow, the length scale $\ell_{u,\text{peak}}$ (corresponding to the energy spectrum peak) appears reasonably independent on the Ekman number, consistent with a large-scale magnetostrophic balance.

In order to assess that these simulations offer a sensible approximation to the magnetostrophic limit, the Elsasser number Λ is reported in figure 9a as a function of the combination $\widetilde{\text{Ra}} = \text{Ra}q$. We also report the modified Elsasser number Λ' as a function of $\widetilde{\text{Ra}}$ in figure 9b. As the field increases with Rm in these simulations, the modified Elsasser number presents a narrower range of variations than the Elsasser number. The first important observation in the strong-dipolar state is that indeed, whereas the Elsasser number is larger than unity and exhibits a clear variation with $\widetilde{\text{Ra}}$, the modified Elsasser number is much closer to unity for all the simulations in the strong-dipolar state (whereas a wide disparity can be observed in both plots for the weak-field state, though with a narrower range in the case of the modified Elsasser number).

The second essential information, is that despite the variations in E , E_η , and q all the strong-dipolar points appear to sit on a single curve. They are only (or almost only)

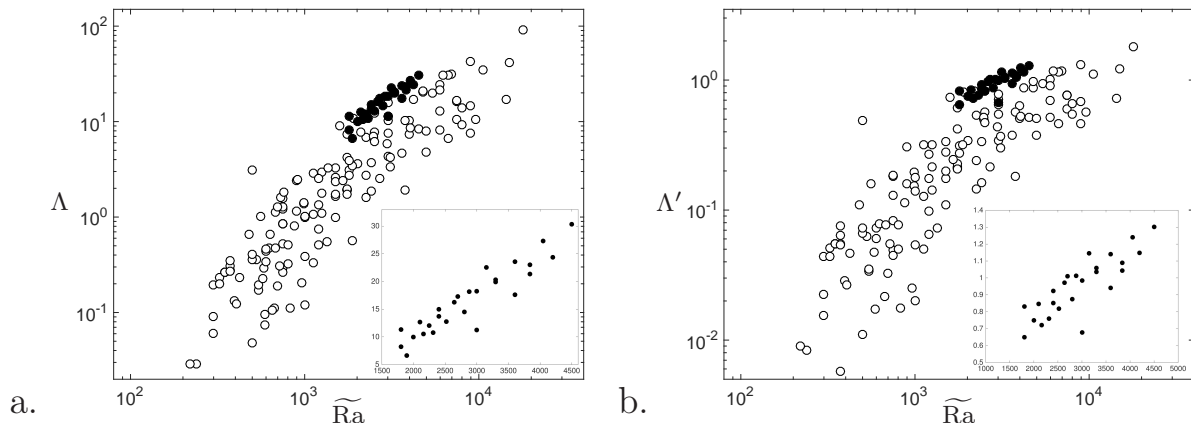


Figure 9. Strength of the magnetic field, as measured by (a) the Elsasser number Λ , (b) the modified Elsasser number Λ' , both as a function of the modified Rayleigh number $\widetilde{\text{Ra}}$, in the weak-dipolar regime (circles) and in the strong-dipolar regime (bullets). The insets present an enlarged representation of dynamos in the strong-dipolar state.

functions of $\widetilde{\text{Ra}}$. This vindicates the scenario of Dormy (2016) that these dynamos are approaching a dominant magnetostrophic balance.

A key prediction on the strong-dipolar branch is that the kinetic energy should be significantly lower than the magnetic energy. This contrasts with the strongly inertial regime in which equipartition is eventually expected. Because of the smallness of the magnetic Ekman number E_η in (1), the magnetic energy E_M should here be much larger than the kinetic energy E_K . We report in figure 10 the evolution of the ratio of the kinetic energy E_K over the magnetic energy E_M as a function of the inverse Ekman number for the three dynamo states discussed in this article. This quantity varies significantly in the weak-dipolar state (see figure 10a). It is less than unity for most models, but no clear trend with the Ekman number can be emphasised. In the multipolar-fluctuating state, the field is generally weaker, while the driving by buoyancy is stronger, as a result, most of these dynamos are characterised by a ratio larger than unity (see figure 10b). In figure 10c, the strong-dipolar models exhibit a clear and systematic decrease of this ratio with the inverse Ekman number. They always correspond to lower values of this ratio than those achieved in the weak-dipolar state. For the smallest Ekman number considered here, this ratio reaches a value lower than on the two other branches. This contrasts with Yadav et al. (2016) who argue that largely super-critical dynamos are needed to decrease this ratio (a result which is however most likely correct on the weak-field branch).

Of course, viscous forces are still present in the strong-dipolar state simulations. Their importance can be quantified by considering, as we did for the weak and multipolar states, the fraction of viscous dissipation. The ratio of the energy being dissipated by viscous forces to the total energy dissipation (viscous and ohmic) should vanish as one approaches the magnetostrophic limit. Figure 11 presents the evolution of the ratio f_ν as a function of various parameters. Figure 11a shows f_ν as a function of the modified

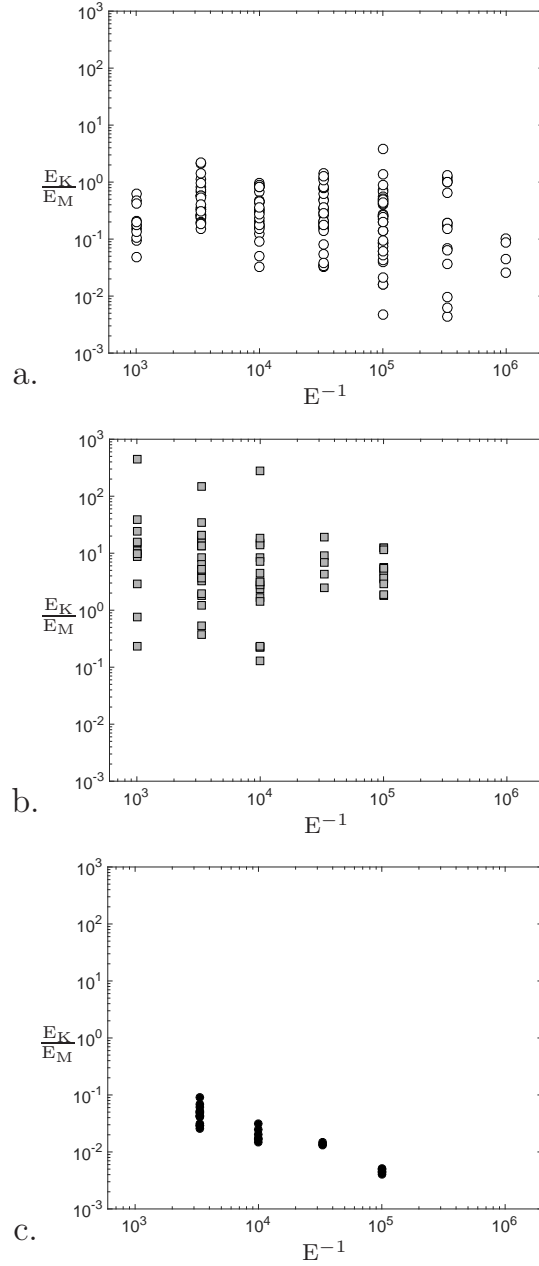


Figure 10. Ratio of the kinetic energy E_K over the magnetic energy E_M as a function of the inverse Ekman number, for (a) weak-dipolar, (b) fluctuating-multipolar and (c) strong-dipolar dynamo states.

Elsasser number Λ' . It highlights that the strong-dipolar state simulations span over a wide range of f_ν . While the viscous dissipation never amounts to more than 50% of the total dissipation, this is a very significant variation. It is then enlightening to represent f_ν as a function of the inverse Ekman number. This graph, represented in figure 11b, shows that, for those dynamos that are in the strong-dipolar state, the fraction of viscous dissipation indeed vanishes as the Ekman number decreases. So that most of the energy is dissipated via ohmic dissipation for the smaller Ekman numbers considered.

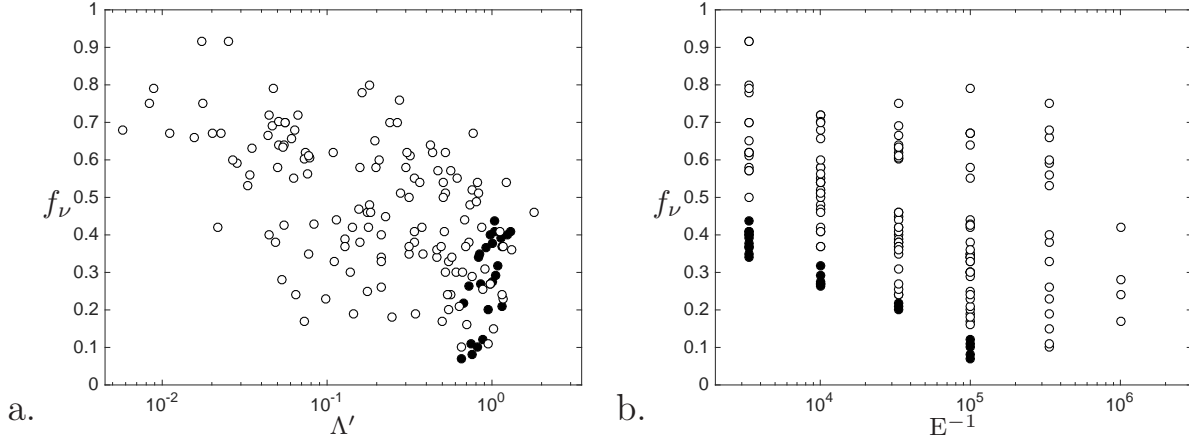


Figure 11. The f_ν parameter as a function of (a) the modified Elsasser number Λ' and (b) the inverse Ekman number E^{-1} , in the weak-dipolar state (circles) and in the strong-dipolar state (bullets).

The relation between figure 10c and figure 11 is subtle. With our choice of non-dimensional form, the kinetic and magnetic energy are expressed, in units of $\Omega\rho\eta L^3$, as

$$E_K = \frac{E_\eta}{2} \int \mathbf{u}^2 dV, \quad E_M = \frac{1}{2} \int \mathbf{B}^2 dV. \quad (11)$$

If our choice of units yields order one values for the integrals, then the ratio E_K/E_M will vanish as E_η .

If we now form the energy equations, after integration by parts, we get

$$\frac{dE_K}{dt} = \int \text{Ra} \, \mathbf{q} \cdot \mathbf{r} \, dV - \int \nabla \times (\mathbf{u} \times \mathbf{B}) \cdot \mathbf{B} \, dV - E \int (\nabla \times \mathbf{u})^2 dV, \quad (12)$$

$$\frac{dE_M}{dt} = \int \nabla \times (\mathbf{u} \times \mathbf{B}) \cdot \mathbf{B} \, dV - \int (\nabla \times \mathbf{B})^2 dV, \quad (13)$$

The above two equations can be rewritten in a condensed form

$$\frac{dE_K}{dt} = P - L - ED^u, \quad \frac{dE_M}{dt} = L - D^B. \quad (14)$$

The first term on the right of (12) is the energy production term P . In non-magnetic hydrodynamics, this energy has to be entirely dissipated in a statistically steady state by the last term on the right-hand-side of (12), i.e. the viscous dissipation ED^u . In magnetohydrodynamics, however, the second term on the right-hand-side of (12), L , allows a transfer of energy to the induction equation (it is equal and opposite to the first term on the right of (13)), where the energy can be ohmically dissipated via the last term in (13), D^B . Equation (14) stresses that $f_\nu = ED^u/(ED^u + D^B)$ vanishes in the limit of small Ekman numbers.

7. Conclusion

We discussed the different dynamo states obtained in numerical models of the Geodynamo. We show that at least three distinct states, characterised by different forces

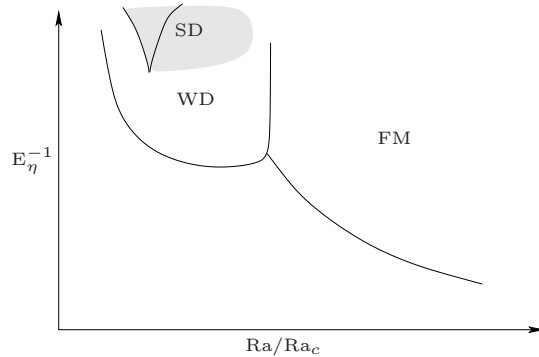


Figure 12. Phase-diagram illustrating, for a given Ekman number, the three different dynamo states observed in numerical simulations of the Geodynamo, namely the weak-dipolar (WD), the fluctuating-multipolar (FM) and the strong-dipolar (SD) states. The cusp indicates the region of bistability between the WD and the SD states. The grey shaded region marks the explored strong-dipolar state.

balances can be highlighted in the available databases of numerical dynamos. These are represented on a schematic phase-diagram at fixed Ekman number on figure 12. The question of the most relevant choice of E_η at a given E is a difficult one. Dormy (2016) suggested that the ratio of these two small parameters should be determined through a distinguished limit, instead of systematically trying to maximise E_η at a given E (i.e. minimise Pm).

It should be noted that the distinguished limit advocated above consists in relating the two small parameters E_η and E in the limiting process, with the ratio $E/E_\eta \equiv Pm$ vanishing in the limit. This contrasts with an alternative approach, which consists in dropping the inertial term, either entirely, or for the non-zonal terms only (Glatzmaier & Roberts 1995, Jones & Roberts 2000, Hughes & Cattaneo 2016), which amounts to an infinite Pm limit.

The first dynamo state (WD), and probably the most documented one, corresponds to a state in which viscosity is entering the main balance, and influencing the convection length-scale. It does not mean to say that these dynamos correspond to a pure “VAC” (Viscous-Archemedian-Coriolis) balance. Other terms, such as inertial effects or Lorentz force, obviously affect the solution. The second state (FM), originally highlighted by Kutzner & Christensen (2002), corresponds to a state in which inertial forces became strong enough so that the Rossby radius became comparable with the convection length scale. In this state the dipolar component no longer dominates the solution, and the field is referred to as multipolar. The third state (SD), introduced by Dormy (2016), is characterised by a runaway field growth from the weak state, due to a cusp catastrophe in the bifurcation diagram. This state appears to correspond to the magnetostrophic force balance anticipated in the Earth’s core. Of course, viscous effects, and inertial effects are still present, but they do not enter the leading order balance.

As the co-existence of the weak and the strong-dipolar states for a given set of parameters (bistability) is associated with the occurrence of a fold in the bifurcation

diagram due to a cusp catastrophe, some models obtained at values of $\text{Pm} = E/E_\eta$ below the appearance of this catastrophe will necessarily share some properties of the strong-dipolar state.

The strong-field state can only be achieved in numerical models so far by adopting a large value of $\text{Pm} = E/E_\eta$. This is only due to computational limitations, and this ratio can be decreased, following a distinguished limit as advocated in Dormy (2016).

Key issues remain, such as: whether dynamo action can be observed for Ra/Ra_c lower than unity. This analytical prediction on the strong-field branch has so far never been reproduced in numerical models – whether the point at which the cusp catastrophe occurs indeed decreases to lower values of $\text{Pm} = E/E_\eta$ as E is decreased – whether a transition from the strong-dipolar state to the fluctuating-multipolar state can be observed for larger forcing. Further studies will undoubtedly be useful to address such open issues.

Appendix A. Numerical data

Table A1. Direct Numerical Simulations performed in the strong-dipolar state.

$\widetilde{\text{Ra}}$	Nu	$\ell_{u\text{vort}}$	$\ell_{u\text{CA06}}$	$\ell_{u\text{peak}}$	ℓ_B	Rm	Λ	E_K/E_M	f_ν
		$E = 3 \times 10^{-4}$		$E_\eta = 2.50 \times 10^{-5}$		q = 12			
1800	1.50	0.0696	0.4760	0.7854	0.0817	167	11.32	0.0312	0.34
2100	1.60	0.0700	—	—	0.0733	205	12.70	0.0410	0.35
2400	1.68	0.0674	0.4586	0.7854	0.0712	228	15.00	0.0433	0.37
2700	1.85	0.0647	0.4425	0.7854	0.0648	265	17.32	0.0503	0.38
3000	1.92	0.0651	0.3653	1.0472	0.0617	300	18.22	0.0617	0.40
3300	2.04	0.0638	0.3530	1.0472	0.0584	330	19.92	0.0691	0.41
3840	2.23	0.0622	0.3653	0.7854	0.0526	389	21.35	0.0900	0.44
		$E = 3 \times 10^{-4}$		$E_\eta = 1.67 \times 10^{-5}$		q = 18			
1890	1.23	—	0.4987	—	—	145	6.60	0.0262	1.00
2250	1.38	—	0.4553	—	—	207	12.00	0.0289	1.00
3150	1.55	0.0655	—	—	0.0690	285	22.50	0.0295	0.37
3600	1.71	0.0648	0.4189	—	0.0595	348	23.60	0.0428	0.39
4050	1.84	0.0632	—	—	0.0555	396	27.27	0.0479	0.40
4500	1.93	0.0622	0.3977	0.7854	0.0533	438	30.35	0.0527	0.41
		$E = 1 \times 10^{-4}$		$E_\eta = 8.33 \times 10^{-6}$		q = 12			
2160	1.45	0.0528	0.3927	0.6283	0.0711	205	10.50	0.0165	0.26
2400	1.60	0.0508	—	—	0.0671	240	13.72	0.0175	0.27
2640	1.76	0.0429	—	—	0.0620	270	16.25	0.0148	0.27
2880	1.83	0.0487	0.3452	0.6283	0.0603	298	18.20	0.0206	0.28
3300	1.95	0.0478	0.3173	0.7854	0.0564	341	20.35	0.0248	0.29
3840	2.21	0.0455	0.2964	0.6283	0.0502	422	23.05	0.0319	0.32
		$E = 3 \times 10^{-5}$		$E_\eta = 3.00 \times 10^{-6}$		q = 10			
3000	1.81	0.0362	0.2732	0.6283	0.0496	335	11.25	0.0148	0.22
3600	2.13	0.0350	0.2493	0.6283	0.0474	394	17.60	0.0136	0.20
4200	2.40	0.0332	0.2212	0.6283	0.0467	455	24.40	0.0134	0.21
		$E = 1 \times 10^{-5}$		$E_\eta = 2.00 \times 10^{-6}$		q = 5			
1800	2.00	0.0363	0.2513	—	0.0638	198	8.20	0.0049	0.07
2000	2.17	0.0267	0.2513	—	0.0632	211	10.00	0.0044	0.11
		$E = 1 \times 10^{-5}$		$E_\eta = 1.43 \times 10^{-6}$		q = 7			
2310	1.90	0.0327	0.2474	—	0.0579	246	10.80	0.0040	0.08
2520	2.12	0.0294	0.2310	—	0.0546	285	12.75	0.0046	0.10
2800	2.30	0.0265	0.2137	—	0.0518	320	14.50	0.0051	0.12

Acknowledgements

This work was granted access to the HPC resources of MesoPSL financed by the Region Ile-de-France and the project Equip@Meso (reference ANR-10-EQPX-29-01) of the programme Investissements d’Avenir supervised by the Agence Nationale pour la Recherche. Numerical simulations were also carried out at CEMAG and TGCC computing centres (GENCI project x2013046698).

References

- Braginsky S I & Roberts P H 1995 *Geophys. Astrophys. Fluid Dyn.* **79**, 1–97.
- Childress S & Soward A M 1972 *Phys. Rev. Lett.* **29**, 837–839.
- Christensen U 2010 *Space Sci. Rev.* **152**, 565–590.
- Christensen U & Aubert J 2006 *Geophys. J. Int.* **166**, 97–114.
- de Wijs G A, Kresse G, Vocablo L, Dobson D, Alfe D, Gillan M J & Price G D 1998 *Nature* **392**, 805–807.
- Dormy E 2016 *J. Fluid. Mech.* **789**, 500–513.
- Dormy E & Soward A M 2007 *Mathematical Aspects of Natural Dynamos* CRC Press, Boca Raton.
- Eltayeb I A & Roberts P H 1970 *Astrophys. J.* **162**, 699–701.
- Fautrelle Y & Childress S 1982 *Geophys. Astrophys. Fluid Dyn.* **22**, 255–279.
- Fromang S & Papaloizou J 2007 *A. & A.* **476**, 1113.
- Fromang S, Papaloizou J, Lesur G & Heinemann T 2007 *A. & A.* **476**, 1123.
- Gallagher I & Gérard-Varet D 2016 *INDAM Series, Springer, in press*.
- Glatzmaier G A & Roberts P H 1995 *Physics of Earth and Planetary Interiors* **91**, 63–75.
- Gubbins D 2001 *Physics of Earth and Planetary Interiors* **128**, 3–12.
- Guervilly C, Hughes D W & Jones C A 2015 *Phys. Rev. E* **91**.
- Holme R 2007 in *Treatise on Geophysics, Olson P, ed. 2007.*, Amsterdam: Elsevier **8**, 107–130.
- Hughes D W & Cattaneo F 2016 *Phys. Rev. E* **93**, 061101.
- Jones C A 2011 *Annu. Rev. Fluid Mech.* **43**, 583–614.
- Jones C & Roberts P 2000 *J. Fluid Mech.* **404**, 311–343.
- King E & Buffett B 2013 *Earth and Planetary Science Letters* **371–372**, 156–162.
- Kutzner C & Christensen U 2002 *Physics of Earth and Planetary Interiors* **131**, 29–45.
- Moffatt H K 1978 *Magnetic Field Generation in Electrically Conducting Fluids* Cambridge University Press, Cambridge.
- Morin V & Dormy E 2006 *Phys. Fluids* **18**, 068104.
- Morin V & Dormy E 2009 *Int. J. Mod. Phys. B* **23**(28-29), 5467–5482.
- Olson P & Christensen U C 2006 *Earth Planet. Sci. Lett.* **250**, 561–571.
- Olson P, Christensen U & Glatzmaier G 1999 *J. Geophys. Res.* **104**, 10,383–10,404.
- Oruba L & Dormy E 2014a *Geophys. J. Int.* **198**, 828–847.
- Oruba L & Dormy E 2014b *Geophys. Res. Lett.* **41**, doi:10.1002/2014GL062069.198.
- Roberts P H 1988 *Geophys. Astrophys. Fluid Dyn.* **44**, 3–31.
- Roberts P H & Wu C C 2014 *Geophys. Astrophys. Fluid Dyn.* **108**, 696–715.
- Schrinner M 2013 *MNRASL* **431**, 78–82.
- Schrinner M, Petitdemange L & Dormy E 2012 *Astrophysical Journal* **752**, 121.
- Simitiev R & Busse F 2009 *Eur. Phys. Lett.* **85**, 19001.
- Soward A M 1974 *Phil. Trans. R. Soc. Lond. A* **275**, 611–646.
- Sreenivasan B & Jones C A 2011 *J. Fluid Mech.* **688**, 5–30.
- Taylor J B 1963 *Proc. Roy. Soc. A* **274**, 274–283.
- Wu C C & Roberts P H 2015 *Geophys. Astrophys. Fluid Dyn.* **109**, 84–110.
- Yadav R, Gastine T, Christensen U, Wolk S J & Poppenhaeager K 2016 *PNAS* **113**, 1206512070.

- Zhang K K & Busse F H 1988 *Geophys. Astrophys. Fluid Dyn.* **44**, 33–53.
Zhang K K & Busse F H 1989 *Geophys. Astrophys. Fluid Dyn.* **49**, 97–116.